A Fundamental Plane of Gamma-Ray Pulsars: Observations and Kinetic PIC Models

C. Kalapotharakos[1,2], A. K. Harding[1,3], D. Kazanas[1], Z. Wadiasingh[1]

[1]Astrophysics Science Division, NASA/Goddard Space Flight Center
[2]University of Maryland, College Park UMCP/CRESST)
[3]Los Alamos National Laboratory

Abstract.
The γ-ray pulsar observables, i.e., their total γ-ray luminosity, L_γ , spectral cutoff energy, ϵ_{cut}, stellar surface magnetic field, B_* , and spin-down power $\dot{\mathcal{E}}$, obey a relation of the form L_γ=f(ϵ_{cut}, B_*, $\dot{\mathcal{E}}$), which represents a 3D plane in their 4D log space. Fitting the data of 88 pulsars of the second Fermi pulsar catalog, we show this relation to be $L_\gamma \propto \epsilon_{cut}^{1.18\pm0.24} B_*^{0.17\pm0.05} \dot{\mathcal{E}}^{0.41\pm0.08}$, a pulsar fundamental plane (FP). The observed FP is remarkably close to the theoretical relation $L_\gamma \propto \epsilon_{cut}^{4/3} B_*^{1/6} \dot{\mathcal{E}}^{5/12}$ obtained assuming that the pulsar γ-ray emission is due to curvature radiation by particles accelerated at the pulsar equatorial current sheet just outside the light cylinder. Interestingly, the FP seems incompatible with emission by synchrotron radiation. We have developed 3D kinetic particle-in-cell pulsar magnetosphere models with magnetic-field line dependent particle injection. In these models the γ-ray emission is regulated by the particle injection rate in the separatrix zone that separates the open from the closed lines and the width of this zone. These innovative models reproduce the FP and the γ-ray light curve patterns as these are depicted in the observed by Fermi-LAT radio-lag δ vs. peak-separation Δ correlation. The comparison between the models and the observations sets constraints on the efficiency of the microphysical processes of the pair production. The models also indicate the existence of a population of γ-ray pulsars for lower $\dot{\mathcal{E}}$ values that are below the Fermi-LAT detection capabilities.

Theory

Orbital Exploration

In any electromagnetic field structure, an asymptotic velocity, v_A, is always defined

$$\mathbf{v_A} = \frac{\mathbf{E}\times\mathbf{B} \pm (E_0\mathbf{E} + B_0\mathbf{B})}{E_0^2 + B^2} c$$

$$E_0 B_0 = \mathbf{E}\cdot\mathbf{B}$$
$$E_0^2 - B_0^2 = \mathbf{E}^2 - \mathbf{B}^2$$

Aristotelian Electrodynamics
(Gruzinov 2012; Kelner et al. 2015)

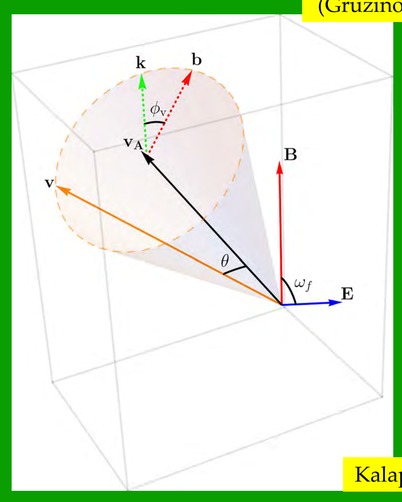

When the particle velocity, v, is close to v_A, the particle emits curvature radiation, while for larger θ values the particle "gyrates" around v_A emitting synchrotron radiation.

Kalapotharakos et al. (2019)

The radius of curvature of the particle trajectory reads

$$R_C = \frac{\gamma_L m_e c^2}{q_e B_{eff}}$$

$$B_{eff} = \sqrt{\left(\mathbf{E} + \frac{\mathbf{v}\times\mathbf{B}}{\mathbf{c}}\right)^2 - \left(\frac{\mathbf{v}\cdot\mathbf{E}}{c}\right)^2}$$

Cerutti, B., Philippov, A. A., & Spitkovsky, A. 2016

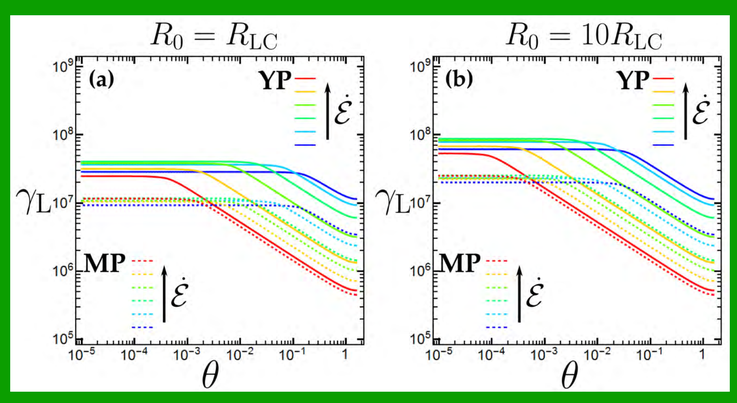

(a) The $\gamma_L$vs. θ relations that reproduce the spectral cutoff energy values, ϵ_{cut}, observed by Fermi-LAT corresponding to the different spin-down power values, $\dot{\mathcal{E}}$ (different colors) for young pulsars (YPs, solid lines) and millisecond pulsars (MPs, dashed lines). These relations assume motion at the light cylinder (LC) and that the radius of curvature corresponding to the asymptotic flow, R_0, is $R_0 = R_{LC}$.
(b) Similar to **(a)** but for $R_0 = 10R_{LC}$.

Recent detections by MAGIC and HESSII of very high-energy emission from the Crab (Ansoldi et al. 2016), Vela (Djannati-Ataï et al. 2017), and Geminga (Lopez et al. 2018) pulsars imply an additional emission component, and inverse Compton (IC) seems to be the most reasonable candidate (Rudak & Dyks 2017; Harding et al. 2018). Thus, the multi-TeV photon energies detected imply very high particle energies ($\gamma_L > 10^7$), which favors CR over SR. (See also the talk of Alice Harding)

γ_L: Lorentz factor

Assumptions
1) Emission at the equatorial current sheet near the light cylinder
2) Radiation Reaction Limit Regime

$$\frac{2q_e^2\gamma_L^4}{3m_e c\, R_C(\theta)} = \frac{q_e \mathbf{v}\cdot\mathbf{E}}{m_e c^2}$$

Taking into account that

$$\epsilon_{cut} = \frac{3}{2} c\hbar \frac{\gamma_L^3}{R_C(\theta)}$$

and trivial scalings

$E_{BLC}B_{LC} \propto \gamma_L^4 R_C^{-2}$ $\quad B_{LC} \propto B_* R_{LC}^{-3} \propto B_* P^{-3}$ $\quad \gamma_L \propto \epsilon_{cut}^{1/3} P^{1/3}$
$n_{GJ} \propto B_* P^{-1}$ $\quad E_{BLC} \propto \epsilon_{cut}^{4/3} P^{7/3} B_*^{-1}$ $\quad L_{\gamma 1} \propto \epsilon_{cut}^{4/3} P^{-2/3}$
$\dot{\mathcal{E}} \propto B_*^2 P^{-4}$

CR → $R_C \propto R_{LC} \propto P$ → $L_\gamma \propto \epsilon_{cut}^{4/3} B_*^{1/6} \dot{\mathcal{E}}^{5/12}$

SR → $R_C \propto r_g \propto \gamma_L B_*^{-1} P^3$ → $L_\gamma \propto \epsilon_{cut} \dot{\mathcal{E}}$

Kalapotharakos et al. (2019)

L_γ: total γ-ray luminosity
P: pulsar period

Observations

Considering 88 young and millisecond pulsars from the second pulsar Fermi catalog (Abdo et al. 2013), we found

$$L_\gamma = 10^{14.2\pm2.3} \epsilon_{cut}^{1.18\pm0.24} B_*^{0.17\pm0.05} \dot{\mathcal{E}}^{0.41\pm0.08}$$

ϵ_{cut}(MeV), B_*(G), L_γ, $\dot{\mathcal{E}}$(erg/s) — **Fermi data**

Kalapotharakos et al. (2019)

which is remarkably close to the relation corresponding to CR

Ploeg et al. (2020), independently confirmed this results working only on the population of millisecond pulsars

$$L_\gamma \propto \epsilon_{cut}^{1.2\pm0.3} B_*^{0.1\pm0.4} \dot{\mathcal{E}}^{0.5\pm0.1}$$

The fundamental plane relation describes a 3D plane embedded in a 4D space.
Thus, in order to visualize the fundamental plane, we appropriately combined the variables

$x = B_*^{1/6} \dot{\mathcal{E}}^{5/12}$
$y = \epsilon_{cut}^{4/3}$
$z = L_\gamma$

The two drawn planes correspond to the theoretical relation for CR and the fitting from the Fermi data. The two planes are remarkably close to each other.

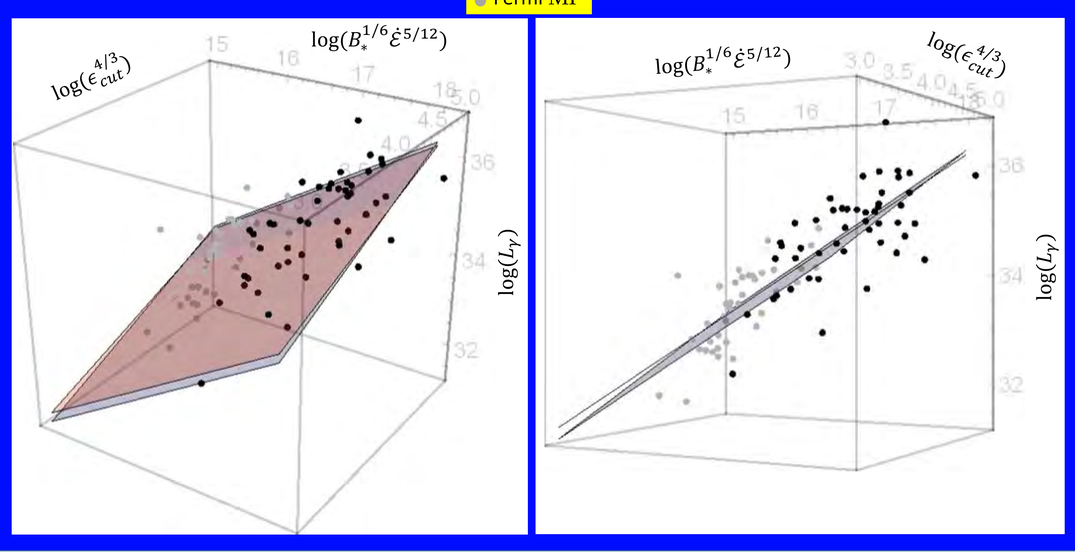

3D Kinetic Particle in Cell Models

We run our simulations of kinetic PIC pulsar magnetosphere models in Pleiades and Discover supercomputers of NASA using our recently developed relativistic PIC code C-3PA (Kalapotharakos et al. 2018; Kalapotharakos et al. 2021, in prep.).

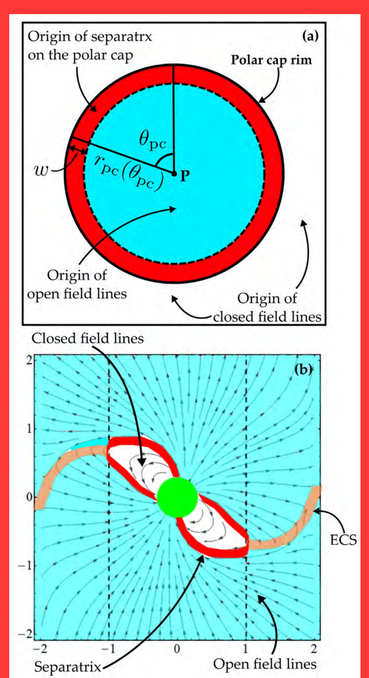

Separatrix injection model

The γ-ray pulsar radiation is mainly regulated by

1. **The particle injection rate $\mathcal{F}_s$ along the separatrix**
2. **The width w of the separatrix zone**

Kalapotharakos et al. (2021, in prep)

Requirements

The particle injection rate along the open and the closed field-lines is not very small. ($> 5\mathcal{F}_{GJ}^0$)
However, it is not necessary to be high. ($< 10\mathcal{F}_{GJ}^0$)

We ran a series of separatrix injection (SI) models for different inclination angles, α, and for a range of $\mathcal{F}_s$ and w values. We identified as optimum the models that reproduce the ϵ_{cut} values observed by Fermi-LAT

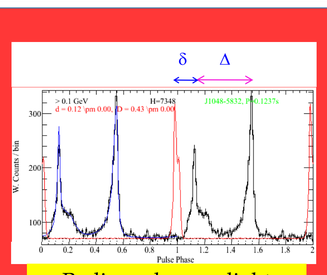

Assuming that the radio pulse originates near the magnetic pole near the stellar surface, the γ-ray light curves corresponding to the optimum SI models reproduce the radio lag, δ vs. peak separation, Δ correlation observed by Fermi-LAT

Radio and γ–ray light curves for pulsar J1048-5832 (from 2PC). Radio-lag (δ) is the phase lag between the radio peak and the first γ–ray peak. Peak-separation (Δ) is the phase difference between the two γ–ray peaks.

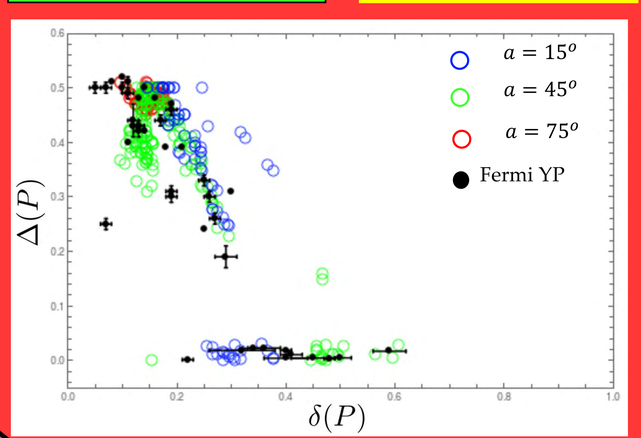

All (optimum and non-optimum) SI models lie on a fundamental plane, which is close to the observed one and the theoretical one corresponding to CR (Kalapotharakos et al. 2021, in prep.)

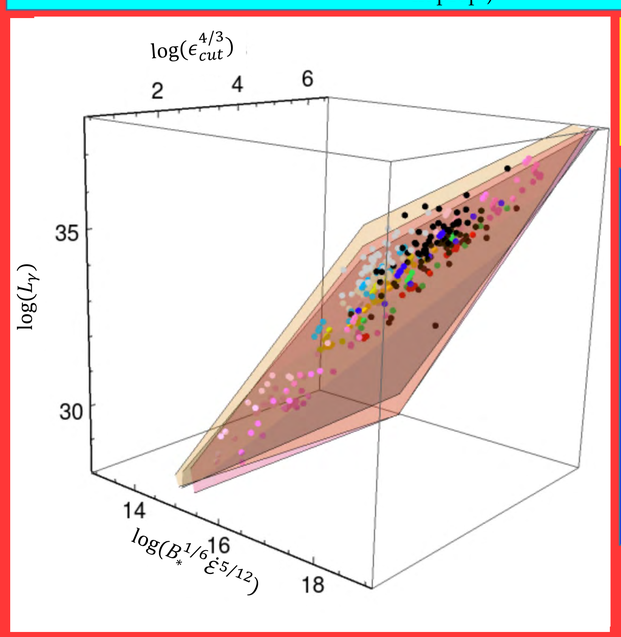

$$L_\gamma \propto \epsilon_{cut}^{1.49\pm0.24} B_*^{0.13\pm0.03} \dot{\mathcal{E}}^{0.40\pm0.06}$$

Optimum PIC SI Models

The Fermi pulsars do not occupy the entire FP but a certain region of it. This uncovers the efficiency of pair production and its dependence on $\dot{\mathcal{E}}$. Moreover, our models indicate the existence of γ-ray pulsars with smaller (than those observed) $\dot{\mathcal{E}}$ values and with smaller ϵ_{cut} values that are below the Fermi detection capabilities.

References

Abdo, A. A., Ajello, M., Allafort, A., et al. 2013, ApJSS, 208, 17 (2PC)
Ansoldi, S., Antonelli, L. A., Antoranz, P., et al. 2016, A&A, 585, A133
Cerutti, B., Philippov, A. A., & Spitkovsky, A. 2016, MNRAS, 457, 2401
Djannati-Ataï, A., Giavitto, G., Holler, M., et al. 2017, in AIP Conf. Ser. 1792, 6th Int. Symp. High Energy Gamma-Ray Astronomy
Harding, A. K., Kalapotharakos, C., Barnard, M., & Venter, C. 2018, ApJL, 869, L18
Kalapotharakos C., Brambilla G., Timokhin A., Harding A.K., Kazanas D., 2018, ApJ, 857, 44
Kalapotharakos C., Harding A.K., Kazanas D., Z. Wadiasingh, 2021, (in prep)
Lopez, M., Schweizer, T., Saito, F., et al. 2018, Proc. ICRC (Lodz), 31
Ploeg H., Gordon C., Crocker R., & Macias O., 2020, JCAP, 12, 035
Rudak, B., & Dyks, J. 2017, Proc. ICRC (Busan), 35, 680